

## Efficient single-photon detection with 7.7 ps time resolution for photon correlation measurements

Iman Esmaeil Zadeh, Johannes W. N. Los, Ronan B. M. Gourgues, Jin Chang, Ali W. Elshaari, Julien Romain Zichi, Yuri J. van Staaden, Jereon P. E. Swens, Nima Kalhor, Antonio Guardiani, Yun Meng, Kai Zou, Sergiy Dobrovolskiy, Andreas W. Fognini, Dennis R. Schaart, Dan Dalacu, Philip J Poole, Michael E. Reimer, Xiaolong Hu, Sylvania F. Pereira, Valery Zwiller, and Sander N. Dorenbos  
ACS Photonics, **Just Accepted Manuscript** • DOI: 10.1021/acsp Photonics.0c00433 • Publication Date (Web): 10 Jun 2020

Downloaded from [pubs.acs.org](https://pubs.acs.org) on June 11, 2020

### Just Accepted

“Just Accepted” manuscripts have been peer-reviewed and accepted for publication. They are posted online prior to technical editing, formatting for publication and author proofing. The American Chemical Society provides “Just Accepted” as a service to the research community to expedite the dissemination of scientific material as soon as possible after acceptance. “Just Accepted” manuscripts appear in full in PDF format accompanied by an HTML abstract. “Just Accepted” manuscripts have been fully peer reviewed, but should not be considered the official version of record. They are citable by the Digital Object Identifier (DOI®). “Just Accepted” is an optional service offered to authors. Therefore, the “Just Accepted” Web site may not include all articles that will be published in the journal. After a manuscript is technically edited and formatted, it will be removed from the “Just Accepted” Web site and published as an ASAP article. Note that technical editing may introduce minor changes to the manuscript text and/or graphics which could affect content, and all legal disclaimers and ethical guidelines that apply to the journal pertain. ACS cannot be held responsible for errors or consequences arising from the use of information contained in these “Just Accepted” manuscripts.

# Efficient single-photon detection with 7.7 ps time resolution for photon correlation measurements

Iman Esmail Zadeh,<sup>\*,†,‡</sup> Johannes W. N. Los <sup>\*,‡</sup>, Ronan B. M. Gourgues,<sup>‡</sup> Jin Chang,<sup>¶</sup> Ali W. Elshaari,<sup>§</sup> Julien Romain Zichi,<sup>§</sup> Yuri J. van Staaden,<sup>¶</sup> Jeroen P. E. Swens,<sup>¶</sup> Nima Kalhor,<sup>‡</sup> Antonio Guardiani,<sup>‡</sup> Yun Meng,<sup>||,⊥</sup> Kai Zou,<sup>||,⊥</sup> Sergiy Dobrovolskiy,<sup>‡</sup> Andreas W. Fognini,<sup>‡</sup> Dennis R. Schaart,<sup>#</sup> Dan Dalacu,<sup>@</sup> Philip J. Poole,<sup>@</sup> Michael E. Reimer,<sup>△</sup> Xiaolong Hu,<sup>||,⊥</sup> Sylvania F. Pereira,<sup>¶</sup> Valery Zwiller,<sup>§,‡</sup> and Sander N. Dorenbos<sup>‡</sup>

<sup>†</sup>*Optics Research Group, ImPhys Department, Faculty of Applied Sciences, Delft University of Technology, Delft 2628 CJ, The Netherlands.*

<sup>‡</sup>*Single Quantum B.V., Delft 2628 CJ, The Netherlands.*

<sup>¶</sup>*Optics Research Group, ImPhys Department, Faculty of Applied Sciences, Delft University of Technology, Delft 2628 CJ, The Netherlands.*

<sup>§</sup>*Quantum Nano Photonics Group, Department of Applied Physics, Royal Institute of Technology (KTH), Stockholm 106 91, Sweden*

<sup>||</sup>*School of Precision Instrument and Optoelectronic Engineering, Tianjin University, Tianjin 300072, China.*

<sup>⊥</sup>*Key Laboratory of Optoelectronic Information Science and Technology, Ministry of Education, Tianjin 300072, China.*

<sup>#</sup>*Medical Physics & Technology, Radiation Science & Technology department, Faculty of Applied Sciences, Delft University of Technology*

<sup>@</sup>*National Research Council of Canada, Ottawa, ON K1A 0R6, Canada.*

<sup>△</sup>*Institute for Quantum Computing and Department of Electrical & Computer Engineering, University of Waterloo, Waterloo, ON N2L 3G1, Canada.*

E-mail: i.esmaeilzadeh@tudelft.nl

## Abstract

A broad range of scientific and industrial disciplines require precise optical measurements at very low light levels. Single-photon detectors combining high efficiency and high time resolution are pivotal in such experiments. By using relatively thick films of NbTiN (8-11 nm) and improving the pattern fidelity of the nano-structure of the superconducting nanowire single-photon detectors (SNSPD), we fabricated devices demonstrating superior performance over all previously reported detectors in the combination of efficiency and time resolution. Our findings prove that small variations in the nanowire width, in the order of a few nanometers, can lead to a significant penalty on their temporal response. Addressing these issues, we consistently achieved high time resolution (best device 7.7 ps, other devices  $\sim$ 10-16 ps) simultaneously with high system detection efficiencies (80 – 90%) in the wavelength range of 780-1000 nm, as well as in the telecom bands (1310-1550 nm). The use of thicker films allowed us to fabricate large-area multi-pixel devices with homogeneous pixel performance. We first fabricated and characterized a  $100 \times 100 \mu\text{m}^2$  16-pixel detector and showed there was little variation among individual pixels. Additionally, to showcase the power of our platform, we fabricated and characterized 4-pixel multimode fiber-coupled detectors and carried out photon correlation experiments on a nanowire quantum dot resulting in  $g^2(0)$  values lower than 0.04. The multi-pixel detectors alleviate the need for beamsplitters and can be used for higher order correlations with promising prospects not only in the field of quantum optics, but also in bio-imaging applications, such as fluorescence microscopy and positron emission tomography.

## Keywords

Superconducting Nanowire Single-Photon Detector, High time resolution, Multi-pixel detectors, Photon correlation, quantum optics.

## Introduction

1  
2  
3  
4  
5  
6 SNSPDs have already pushed the limits in several fields such as CMOS testing,<sup>1</sup> biomedical  
7 imaging,<sup>2</sup> laser ranging,<sup>3</sup> and quantum communication.<sup>4,5</sup> These detectors have unparalleled  
8 performance: high efficiency ( $>90\%$ ),<sup>6-8</sup> time resolution ( $<3$  ps for a short nanowire section<sup>9</sup>  
9 and  $<15$  ps for complete efficient detectors<sup>8,10</sup>), and count-rate.<sup>11</sup> Yet, for studying fast  
10 phenomena in chemistry, biology, physics, efficient detectors with better timing jitter are  
11 required. Although direct high time-resolution measurements are possible, for example with  
12 streak cameras, they suffer from low detection efficiencies, typically  $< 10\%$ , high dark count  
13 rates and are limited to viewing a narrow time window,<sup>12,13</sup> moreover they are bulky and  
14 costly. Meanwhile, the fiber coupled SNSPDs allow for a cost efficient integration of many  
15 high performance detectors in a single cryostat. Here we demonstrate SNSPDs made of  
16 relatively thick NbTiN films with superior time resolution and high efficiencies. Moreover,  
17 we show large area sensors using arrays of SNSPDs with minimal variation in performance  
18 over the array. In addition to optical imaging applications, this technology could be used  
19 to read-out fast scintillators, potentially enabling the detection of ionizing radiation with  
20 unprecedented time resolution, which is of great interest for time-of-flight positron emission  
21 tomography.<sup>14</sup> We showcase our platform by carrying out photon correlation measurements  
22 using a multi-pixel multimode fiber-coupled detector.  
23  
24  
25  
26  
27  
28  
29  
30  
31  
32  
33  
34  
35  
36  
37  
38  
39

40 We fabricate our detectors from sputtered NbTiN films on top of a  $\text{SiO}_2/\text{Au}$  cavity or  
41 a distributed Bragg reflector. To achieve the highest possible absorption in the supercon-  
42 ducting layer, increasing the critical current and reducing kinetic inductance (and hence the  
43 deadtime), thicker films are desirable.<sup>8</sup> On the other hand, increasing the film thickness leads  
44 to a higher energy gap<sup>15</sup> and possible reduction of the kinetic energy of the quasiparticles due  
45 to less available energy following an excitation. Therefore, for such films, it is challenging  
46 to reach saturation of the internal efficiency, and hence, both the material properties of the  
47 film and the fabrication uniformity of the SNSPD nanowire meander have to be controlled.  
48  
49  
50  
51  
52  
53  
54  
55  
56  
57  
58  
59  
60

## Fabrication and Characterization

Magnetron sputtering was used to deposit the films and similar to ref.<sup>16</sup>, we varied the sputtering parameters to achieve both high current and saturation of internal efficiency at the wavelength of 820 nm (we also optimized films and fabricated high performance devices optimized for the telecom wavelength range, see supporting information). Figure1(a) represents, similar to ref.<sup>16</sup>, the measured internal efficiency (the saturation plateau,  $\frac{I_c - I_{sat}}{I_c}$ ) for detectors made from 9 nm thick films with different partial Nb contents. As it can be observed, all detectors with different Nb fractions show a saturation plateau, therefore, to enhance the signal to noise ratio and hence the timing jitter, we based our choice on the films which provided the highest critical current density and highest sheet resistance. All devices, unless mentioned, are fabricated from films with a Nb partial ratio of 0.85 (Nb<sub>0.85</sub>Ti<sub>0.15</sub>N). This composition yields detectors which not only have a high critical current density and a long saturation plateau (at the studied wavelength), but also can be operated at higher temperatures<sup>17</sup> and are compatible with large scale integrated nanophotonics.<sup>18</sup> We optimized our fabrication recipe and fabricated detectors with high uniformity. High resolution SEM images of sample devices are shown in Figure1(b).

Localized inhomogeneities are known to limit the critical current of SNSPDs made out of thin crystalline films (such as NbN and NbTiN).<sup>19</sup> We investigate whether the inhomogeneities can also affect our thicker NbTiN films by embedding short constrictions in the meandering detector as shown in Figure1(c). The main SNSPD meander had a width of 100 nm and the constriction was 70 nm wide. The length of this constriction was varied from 50 nm to 5  $\mu$ m (always a straight section wire with no bends) and we measured their critical currents at several temperatures in the range of 4.2 K to 8.5 K (Figure1(d)). We did not observe any significant degradation of critical current with the increase of constriction length. Furthermore, many of our fabricated shorter SNSPDs ( $\sim 400 \mu$ m long) and longer SNSPDs ( $\sim 4$  mm long) showed similar critical currents.

It has been shown that local variation of nanowire width can influence the time resolution

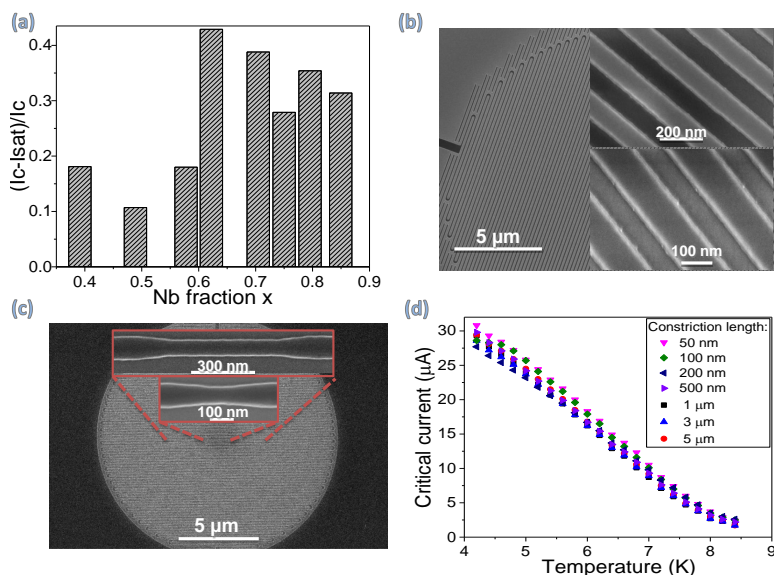


Figure 1: (a) Saturation of internal efficiency for sputtered, 9 nm thick, films of  $Nb_xTi(1-x)N$  versus their Nb fraction at 830 nm. (b) SEM images of devices fabricated and optimized for the wavelength range of 800-900 nm. Top and bottom insets show devices with filling factor of  $\sim 0.55$  and 0.6, respectively. (c) Meander with a short constricted region. The main nanowire has a width of 100 nm and the width in the constriction region is 70 nm. The constriction length varies from 50 nm to 5000 nm and is always a straight section (not including bends). (d) Critical currents of devices described in (c) versus temperature. No significant change of critical currents was observed when changing the constriction length.

of SNSPDs.<sup>20</sup> To investigate the relevance of these local variations on the time resolution of our devices, we fabricate and characterize SNSPDs sectioned in two regions with different nanowire widths. Figure 2(a) is an illustration of such a two sectioned SNSPD and Figure 2(b) shows an SEM image of a fabricated device with 70 nm and 77 nm wide sections. We designed the device so that the length of 77 nm wide section is about  $\sim 7.7$  times longer than the 70 nm wide section. The ratio between the length of different sections were experimentally chosen to signify the influence of widths variation and also the change in the profile of time response with respect to the bias current. We measure the SNSPD jitter by correlating the SNSPD pulses (start signal) with that of a pulsed laser (1060 nm, 5.08 ps, 48.6 MHz) as stop signal, shown in Figure 2(c). Two distinct peaks can be observed, corresponding to the two different meander sections. We ascribe the peak on the right side to the 70 nm wide section because of its higher resistance which leads to faster risetime and hence earlier start

1  
2  
3 signal. The fast risetime also leads to a narrower distribution since noise jitter is inversely  
4 proportional to the slope. The left side peak is ascribed to the 77 nm wide section which  
5 has the lower resistance and hence the late start signal. We also investigated the temporal  
6 profile of detection events as a function of bias current, as shown in Figure 2(d).  
7  
8  
9

10  
11 To better understand the bias-current-dependent histograms of our two-section device, we  
12 numerically simulated these histograms including electronic-noise-induced timing jitter,<sup>21,22</sup>  
13 geometric timing jitter,<sup>23</sup> and inhomogeneity-induced timing jitter,<sup>24</sup> see supporting infor-  
14 mation for details. As presented in Figure 2(e), the simulated histograms show the features  
15 of double peaks which were also observed experimentally (Figure 2(d)). The system detec-  
16 tion efficiency of each section determines the area under each peak, and therefore, is the  
17 major factor affecting the amplitude of each. As the system detection efficiency of the two  
18 sections both vary with the bias current, the relative areas of these two peaks also vary as a  
19 function of the bias current. The separation between the two peaks is the difference of time  
20 delays. We see that the simulated separations between the two peaks are larger than the  
21 measured results; so that at low bias level, two distinct peaks are obtained in simulation,  
22 as opposed to a main peak with a shoulder as observed experimentally. This discrepancy  
23 is mainly due to the fact that simulated leading edges of these time-domain pulses do not  
24 perfectly match the experimental results (see supporting information).  
25  
26  
27  
28  
29  
30  
31  
32  
33  
34  
35  
36  
37  
38

39 Nanofabrication of SNSPDs can introduce imperfections; the nanowire width may vary  
40 along the meander for a number of systemic and fabrication issues. A common factor is the  
41 proximity effect during electron beam lithography. The proximity effect can cause center  
42 areas of the detector to have a wider or narrower width (depending on the tone, thickness  
43 and chemistry of the ebeam resist as well as the properties of the substrate, see supporting  
44 information for examples of proximity effect simulations), resulting in a similar behaviour  
45 to that of Figure 2(c). However, due to the limitations of the experimental setups, it is not  
46 always possible to resolve the peaks, yet we observed two distinct peaks in the temporal  
47 response of devices with a width difference as low as 2 nm (supporting information). It  
48  
49  
50  
51  
52  
53  
54  
55  
56  
57  
58  
59  
60

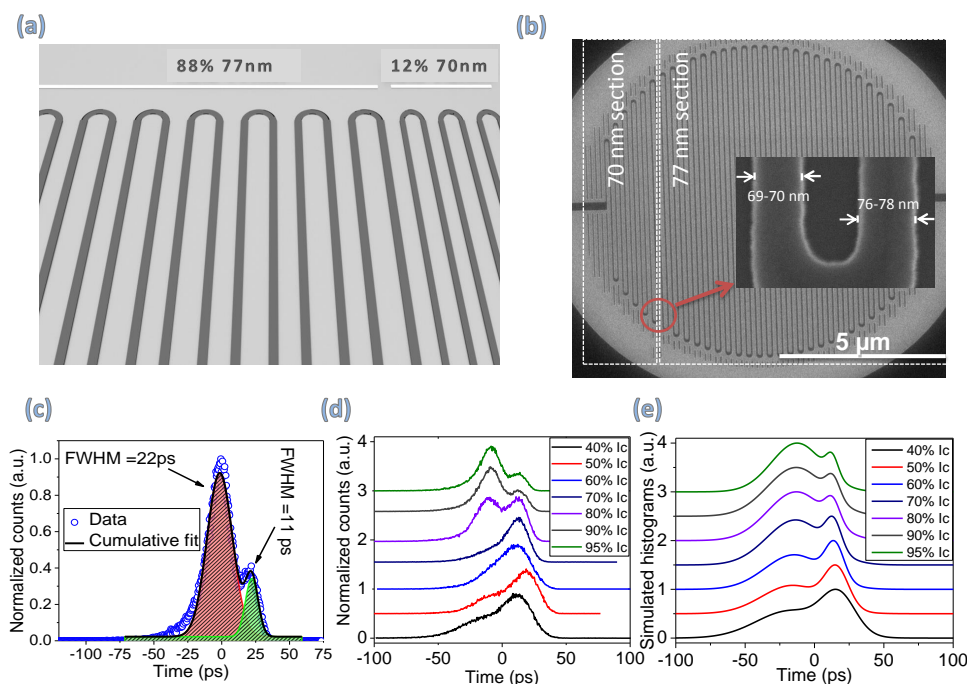


Figure 2: (a) Schematic illustration of a two section SNSPD: having  $\sim 12\%$  (of its area) 70 nm nanowire width and  $\sim 88\%$  a width of 77 nm. (b) SEM image of a two section SNSPD. The inset shows a magnified high resolution SEM of the transition between 70 and 77 nm. The measured values were in good agreement with the design (also see supporting information for more SEM images). (c) Time jitter for the two-section SNSPD, at a bias current equivalent to 95% of critical current. Two distinct peaks can be observed, which correspond to the two different meander sections. (d) Time jitter measurements for the same detector at various bias currents. It can be observed that at lower biases the detections mostly occur in the 70 nm section (higher internal saturation) while at higher biases it is dominated by 77 nm section (larger surface area). This difference depends on the degree of saturation of each section. (e) Simulated correlation histograms at different bias currents.

should be noted that if the device has more gradual widths variations (which is plausible considering the profile of proximity effects), instead of distinct peaks, one would expect a single broad peak. Proximity effects can be accounted and compensated for, however, it requires simulation, optimization and verification for each single pattern, resist, and every electron beam lithography system. As our simulation suggests (supporting information) and from the literature,<sup>25</sup> that it is possible to significantly reduce the PE using thinner ebeam resists. We tuned the resist thickness (for negative tone, 25-30 nm XR1541, and for positive tone 90-100 nm PMMA/AR-P 6200.04), the reactive ion etching chemistry (12.5 sccm  $SF_6$ ,

1  
2  
3 3.4 sccm  $O_2$ , and a process pressure of  $\sim 4\mu\text{bar}$ ), and etching power and time (50 W and  
4 45 seconds), and fabricated 70-100 nm wide nanowires made out of 10-13 nm thick films.  
5 The resulting detectors showed saturated internal efficiency in the wavelength range of 400-  
6 1064 nm. Note that the top section of the film has 0.5-1.5 nm oxidized layer,<sup>26</sup> preventing  
7 it from further oxidation. For high efficiency and high time resolution telecom detectors we  
8 used slightly thinner films (8.5-9.5 nm). For all fiber-coupled devices, unless otherwise clearly  
9 stated, the nanowire width and filling factor were 70 nm and 0.5, respectively.  
10  
11

12 For the measurement of high performance detectors, we packaged and characterized the  
13 detectors in a standard setup similar to.<sup>8</sup> For efficiency measurements, at each wavelength we  
14 adjusted the input power to 10 nW and then attenuated it by 50 dB, setting an input photon  
15 flux in the range of 200-800 Kcounts/second for visible to telecom wavelength range. For  
16 jitter measurements at low photon fluxes, we used a pico-second pulsed laser (same laser as  
17 was used for characterization of two-section detectors), and we kept the detector count-rate  
18 in the range of 60-100 Kcount/second. Figure 3(a) and 3(b) present the efficiency and jitter  
19 measurement results for a detector optimized for the wavelength range of 880-950 nm (from  
20 a 10 nm thick film), respectively. For other wavelengths we achieved similar performance,  
21 see supporting information. We measured a system detection efficiency of  $> 85(\pm 5\%)$  and  
22 system time resolution of  $9.23 \pm 0.05$  ps (deconvoluted 7.70 ps, see supporting information).  
23 Other devices for this wavelength had SDE of 82-91.5% and time resolution of 9.5-15 ps (see  
24 supporting information). The inset in Figure 3(b) is a logarithmic plot of the data and fit. On  
25 the left side of the jitter measurement data, a small asymmetry and deviation from the fit is  
26 observed. Besides originating from the nanowire width variation, this asymmetry could also  
27 be due to detection in the nanowire bends as reported in.<sup>27</sup> However, in comparison with<sup>27</sup>  
28 our degree of asymmetry is smaller, which most likely is explained by the non uniform  
29 illumination of our device caused by the fact that the fiber coupled detector has a diameter  
30 larger than the mode field diameter of the optical fiber. As a result, the meander bends  
31 are not efficiently illuminated. The asymmetry was stronger when we flood illuminated the  
32  
33  
34  
35  
36  
37  
38  
39  
40  
41  
42  
43  
44  
45  
46  
47  
48  
49  
50  
51  
52  
53  
54  
55  
56  
57  
58  
59  
60

detectors in a free-space setup (in this case, bends were illuminated). To achieve the best time resolution, we triggered the correlator on the steepest part of the pulses rising edge. We also studied the effect of trigger level (varying it from 10% to 80% ) on the value of the FWHM of detector jitter (see supporting information). An increase in the FWHM jitter can be observed, from 15.5 ps to 22.5 ps for a sample detector. This is likely to be caused by reduced signal to noise ratio (slower rise time or higher noise level).

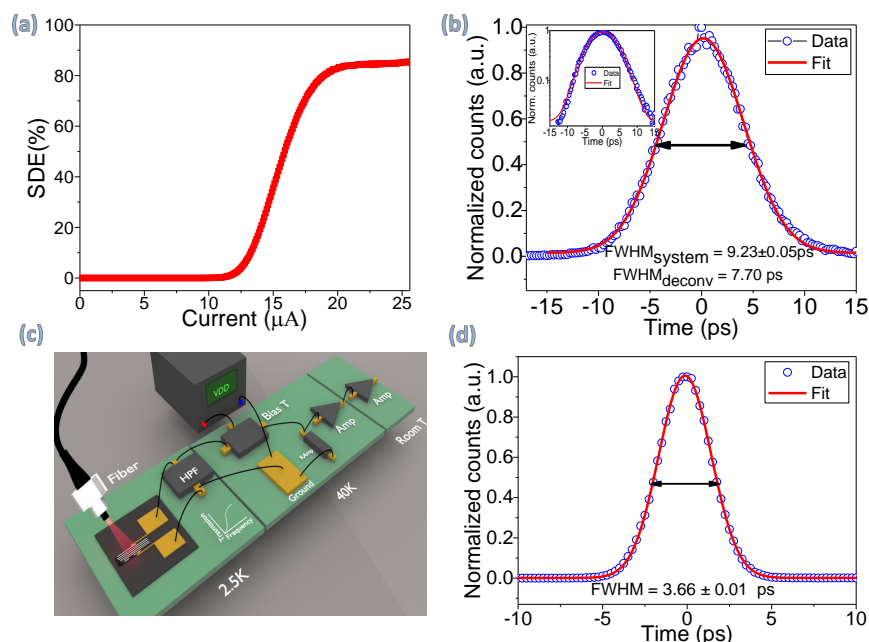


Figure 3: (a) Efficiency vs bias current for a detector at 915 nm, the peak efficiency is  $85 \pm 4.5\%$  (b) Jitter measurement for the same detector as part (a), the FWHM of the jitter, obtained from a Gaussian fit, is  $9.23 \pm 0.05$  ps. Considering the duration of the laser pulses (5.08 ps) and neglecting the contribution from the correlator and photodiode ( $\sim 2.5$  ps), we obtain an SNSPD instrument response function of 7.70 ps (see supporting information). (c) An illustration of the SNSPD readout circuit used for high photon fluxes. (d) At higher photon fluxes using our new readout circuit, from the fit to the data we calculated a system time resolution of  $3.66 \pm 0.01$  ps (please note, this measurement was carried out on the device shown in S1(a)).

We also investigated the count-rate dependence of the jitter (see supporting information). We observed that at low count-rates (below  $0.1 \times$  laser repetition-rate), the SNSPD time jitter exhibits a typical single Gaussian distribution. However, as the count-rate increases, other peaks start to appear in the distribution. The observation of these peaks can be

1  
2  
3 explained by the fact that when the bias recovery time of a SNSPD is longer than  $\frac{1}{\text{laser rep. rate}}$ ,  
4 subsequent detection events take place with an under-biased detector while detection events  
5 which are temporally further away would experience normal detection (similar to low count-  
6 rate regime). Therefore, these different cases result in different risetime/signal levels, which  
7 consequently lead to multiple peaks in the jitter measurement.  
8  
9

10  
11 Normally, SNSPDs under high excitation powers latch into the normal mode (they be-  
12 come normal with no recovery to the superconducting mode). By providing a low frequency  
13 path for the SNSPD current to ground, it is possible to operate detectors at higher powers.  
14 Moreover, by using high-bandwidth low-loss coax cables, a low jitter can be achieved. We  
15 use a high pass filter, as shown in Figure 3(c), in series with the detector to allow for high  
16 power operation together with low jitter. The low-pass filter made it possible to operate  
17 the detector with higher powers (1-10 nW). With higher intensity, we make sure that every  
18 single laser pulse is filled with several photons. Therefore, the risetime and signal level stays  
19 constant for all detection events and the temporal distance between photons become shorter.  
20 Moreover, at these high powers, any SNSPD intrinsic/geometry contribution to the jitter is  
21 negligible as only the fastest events trigger the correlator. To this end the only limit we  
22 observed was the electrical noise and limited bandwidth of the amplifiers. The result of  
23 time jitter measurement with multi-photon excitation ( $>100$  photons per pulse) is shown in  
24 Figure 3(d), demonstrating a very high time-resolution of 3.66 ps ( $<3$  ps after decoupling  
25 the contributions from the correlator and the photodiode, see supplementary).  
26  
27  
28  
29  
30  
31  
32  
33  
34  
35  
36  
37  
38  
39  
40  
41  
42  
43  
44

## 45 Quantum Correlation with a Multi-Pixel SNSPD

46  
47  
48 Many optical experiments in chemistry, biology and material science deal with scattered light  
49 which cannot be efficiently collected and coupled into single mode optical fibers. Therefore,  
50 sensors with large active areas are required. SNSPDs with large active areas have gained  
51 attention in the recent years and several works on single pixel<sup>28-31</sup> and multi-pixel devices<sup>32-34</sup>  
52  
53  
54  
55  
56  
57  
58  
59  
60

have been reported. Compared to Multi-pixel devices, Single-pixel large-area devices are less complex and require only one readout channel. However there is a price to pay, since many performance parameters of SNSPDs such as deadtime and jitter and also fabrication yield suffer as the device length is increased. Until now these factors have limited the work of extending the size of single-pixel SNSPDs.

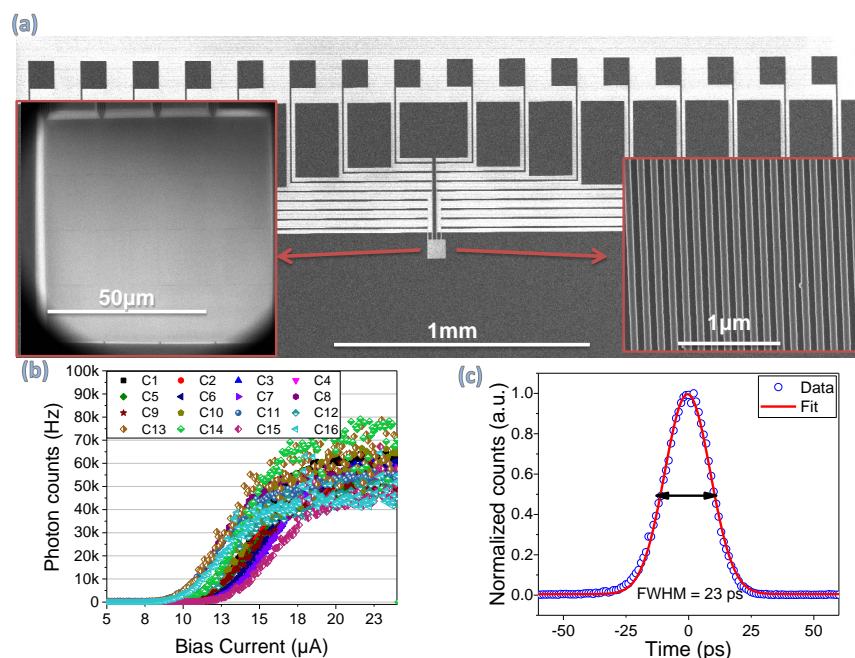


Figure 4: (a) SEM image of a fabricated 16 pixel SNSPD array covering an area of  $100 \times 100 \mu\text{m}^2$  (pixel size  $25 \times 25 \mu\text{m}^2$ ). The two insets show magnified images of the sensor array. (b) Photon count rate versus bias current for different pixels of the SNSPD array. The performance of different pixels are similar and we attribute the small differences in pixels responses to the fact that the data was collected in two cooldown cycles (temperature and illumination variation). Nevertheless, for a bias current  $>20 \mu\text{A}$ , all pixels reach saturation of internal efficiency. (c) Timing jitter measurement for one of the pixels. The measured system jitter of 23 ps is  $>25$  times better if we only consider the reported geometrical jitter in other platforms.

For multi-pixel SNSPD arrays, as the operation point and performance of individual pixels are usually not uniform, scaling these sensors also pose practical implementation challenges. Here we demonstrate, using our thick NbTiN films, multi-pixel arrays with small variations in performance of the pixels. Figure 4(a) show SEM images of a fabricated 16 pixel SNSPD array covering an area of  $100 \times 100 \mu\text{m}^2$  (pixel size  $25 \times 25 \mu\text{m}^2$ ). We measure

1  
2  
3 the photon count rate versus bias current for different pixels of the SNSPD array using a  
4 flood-illumination setup at 670 nm. The results are presented in Figure 4(b). It can be  
5 observed that the performance of all pixels are similar (for a bias current  $>20 \mu A$ , all pixels  
6 reach saturation of internal efficiency) and therefore, a much simpler biasing circuit can be  
7 used. We attribute the small differences in pixels responses to the fact that the data was  
8 collected in two cooldown cycles (cooldown 1: pixels 1-8, cooldown 2: pixels 9-16) and the  
9 temperature and illumination might had small variations (also within one cooldown there  
10 might be small variations in uniformity of illumination, see supporting information). The  
11 measured switching current, within each cooldown, for all but one pixel had a variation  
12 less than 2% (comparable to the precision of our biasing circuit). Only one pixel, due to  
13 a bonding issue, had an oscillatory behavior near the switching current making it difficult  
14 to determine the exact switching current (the highest measured variation for this case was  
15  $\sim 10\%$ ). We also measured the time jitter for some pixels of the array, the results of one  
16 such measurement is provided in Figure 4(c). The measured system jitter of 23 ps for a  
17  $\sim 4.46$  mm long detector is  $>25$  times better than other platforms<sup>35-37</sup> even considering only  
18 the geometrical jitter, which indicates that the electromagnetic field does not have as high  
19 confinement in our platform as detectors made from thinner films (capacitive coupling of  
20 signal between the lines).  
21  
22  
23  
24  
25  
26  
27  
28  
29  
30  
31  
32  
33  
34  
35  
36  
37  
38

39 The multi-element detectors are of particular interest in quantum optics as they provide  
40 direct photon correlation measurements with no need of spatially splitting the beam to differ-  
41 ent detectors. We carry out antibunching measurements using a 4-pixel multimode fiber cou-  
42 pled SNSPD (made from a 9.5 nm wide NbTiN film) on a semiconductor nanowire quantum  
43 dot. These sources have been extensively studied in the literature and have demonstrated  
44 promising performance in terms of clean emission spectra,<sup>38</sup> as entangled photon sources<sup>39</sup>  
45 and for near-unity coupling to fibers.<sup>40</sup> We use a 4-pixel multimode fiber coupled SNSPD  
46 to carry photon correlation measurements on the single-photons generated by a nanowire  
47 quantum dot. SEM image of the detector is shown in Figure 4(a) with the ground pads  
48  
49  
50  
51  
52  
53  
54  
55  
56  
57  
58  
59  
60

1  
2  
3 (G), signal pads (S), and pixel labels (1, 2, 3, 4) highlighted in the figure. Our measurement  
4  
5 setup is illustrated in Figure 4(b), a cryogenically cooled source is excited using a CW laser  
6  
7 (516 nm) and collected photons are filtered using a monochromator (Princeton Instrument  
8  
9 Acton 2750) and are coupled to the detector through a graded index  $50\ \mu\text{m}$  fiber. We con-  
10  
11 duct photon correlation measurements between different pixel pairs of the detector, and the  
12  
13 results for 3 of these pairs are presented in Figure 4(c) (unprocessed data are available in  
14  
15 the supporting information). The measured low value of  $g^2(0)$ , consistent or better than pre-  
16  
17 viously measured  $g^2(0)$  on similar sources,<sup>41</sup> without using any beamsplitter demonstrates  
18  
19 the usefulness and versatility of such detectors.  
20  
21  
22

## 23 Conclusion

24  
25  
26 We demonstrated superconducting nanowire single-photon detectors (SNSPD), fabricated  
27  
28 from NbTiN thick films, combining high time resolution and high efficiencies at the same  
29  
30 time. The influence of fabrication imperfections on the time resolution of SNSPDs was stud-  
31  
32 ied and it was revealed that a small variation in the order of a few nanometer can significantly  
33  
34 influence the timing jitter. We showed that thicker films of NbTiN are less susceptible to  
35  
36 small local material imperfections and therefore, a good candidate to serve as large active  
37  
38 area high performance photonic sensors. A multi-pixel detector was showcased as a quantum  
39  
40 correlator in a Hanbury Brown and Twiss experiment without using a beamsplitter. The re-  
41  
42 sulting low  $g^2(0)$  demonstrates the potential of such devices not only in the field of quantum  
43  
44 optics, but also in the fields such as fluorescence microscopy. Large-area multi-pixel SNSPDs  
45  
46 are furthermore expected to have bright prospects in ultra-fast optical and medical imaging  
47  
48 applications.  
49  
50  
51  
52  
53  
54  
55  
56  
57  
58  
59  
60

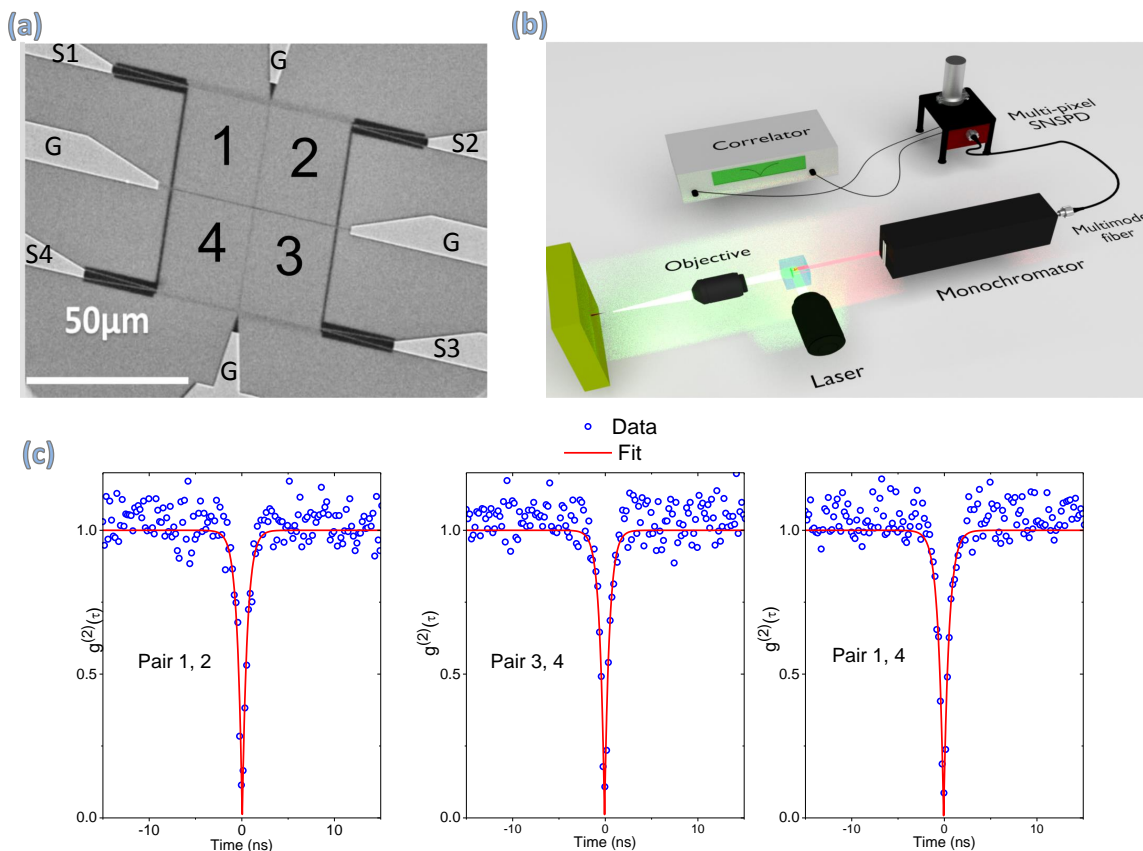


Figure 5: (a) SEM image of a fiber-coupled 4-pixel device covering an area of  $50 \times 50 \mu\text{m}^2$ . (b) Illustration of the photon antibunching measurement setup used to benchmark the 4-pixel detector. (c) Results of photon correlation measurements with three out of six possible pixel pair combinations (complete dataset can be found in supporting information). All pair combinations yield similar outcomes (depending on binning: a  $g^2(0)$  between 0.03 and 0.1) while the fit at time 0 vanishes completely. The difference between the data and the fit is mainly due to timing jitter induced by a path-length difference in the monochromator (see supporting information).

## Funding Sources and Conflict of Interest

I. E. Z., A. W. E., V. Z., D. R. S., and Single Quantum B.v. acknowledge the supports from the ATTRACT project funded by the EC under Grant Agreement 777222. I. E. Z. acknowledges the support of Nederlandse Organisatie voor Wetenschappelijk Onderzoek (NWO), LIFT-HTSM (project 680-91-202). R. B. M. G acknowledges support by the European Commission via the Marie-Sklodowska Curie action Phonsi (H2020-MSCA-ITN-642656). A. W. E. acknowledges support from the Swedish Research Council (Vetenskapsrådet) Starting

1  
2  
3 Grant (ref: 2016-03905). V. Z. acknowledges funding from the Knut and Alice Wallenberg  
4 Foundation Grant "Quantum Sensors", and support from the Swedish Research Council  
5 (VR) through the VR Grant for International Recruitment of Leading Researchers (Ref  
6 2013-7152) and Research Environment Grant (Ref 2016-06122). Y. M., K. Z., and X. H. ac-  
7 knowledge the support from Natural Science Foundation of Tianjin City (19JCYBJC16900).  
8  
9  
10  
11  
12  
13  
14

## 15 **Author Contributions**

16  
17  
18 I. E. Z. and J. W. N. L contributed equally to this work.  
19  
20  
21  
22

## 23 **Notes:**

24  
25  
26 The authors declare no competing financial interest.  
27  
28  
29

## 30 **Acknowledgement**

31  
32  
33 The authors would like to thank Dr. Gabriele Bulgarini and Dr. Stephan Steinhauer for the  
34 fruitful discussions.  
35  
36  
37  
38  
39

## 40 **Supporting Information Available**

41  
42  
43 The supporting information includes additional examples of high performance devices (S1),  
44 supplementary information and simulations for detectors' time jitter (S2) as well as further  
45 data on multi-pixel devices(S3).  
46  
47  
48  
49  
50  
51  
52  
53  
54  
55  
56  
57  
58  
59  
60

## References

- (1) Zhang, J. et al. Noninvasive CMOS circuit testing with NbN superconducting single-photon detectors. *Electronics Letters* **2003**, *39*, 1086–1088.
- (2) Pe'er, A.; Bromberg, Y.; Dayan, B.; Silberberg, Y.; Friesem, A. A. Broadband sum-frequency generation as an efficient two-photon detector for optical tomography. *Opt. Express* **2007**, *15*, 8760–8769.
- (3) McCarthy, A.; Krichel, N. J.; Gemmell, N. R.; Ren, X.; Tanner, M. G.; Dorenbos, S. N.; Zwiller, V.; Hadfield, R. H.; Buller, G. S. Kilometer-range, high resolution depth imaging via 1560 nm wavelength single-photon detection. *Opt. Express* **2013**, *21*, 8904–8915.
- (4) Yin, J.; Cao, Y.; Liu, S.-B.; Pan, G.-S.; Wang, J.-H.; Yang, T.; Zhang, Z.-P.; Yang, F.-M.; Chen, Y.-A.; Peng, C.-Z.; Pan, J.-W. Experimental quasi-single-photon transmission from satellite to earth. *Opt. Express* **2013**, *21*, 20032–20040.
- (5) Vallone, G.; Dequal, D.; Tomasin, M.; Vedovato, F.; Schiavon, M.; Luceri, V.; Bianco, G.; Villoresi, P. Interference at the Single Photon Level Along Satellite-Ground Channels. *Phys. Rev. Lett.* **2016**, *116*, 253601.
- (6) Marsili, F.; Verma, V. B.; Stern, J. A.; Harrington, S.; Lita, A. E.; Gerrits, T.; Vayshenker, I.; Baek, B.; Shaw, M. D.; Mirin, R. P.; Nam, S. W. Detecting single infrared photons with 93% system efficiency. *Nat Photon* **2013**, *7*, 210–214.
- (7) Zhang, W. J.; You, L. X.; Li, H.; Huang, J.; Lv, C. L.; Zhang, L.; Liu, X. Y.; Wu, J. J.; Wang, Z.; Xie, X. M. NbN superconducting nanowire single photon detector with efficiency over 90% at 1550 nm wavelength operational at compact cryocooler temperature. *Science China Physics, Mechanics & Astronomy* **2017**, *60*, 120314.
- (8) Zadeh, I. E.; Los, J. W. N.; Gourgues, R. B. M.; Steinmetz, V.; Bulgarini, G.; Dobrovolskiy, S. M.; Zwiller, V.; Dorenbos, S. N. Single-photon detectors combining high

- 1  
2  
3 efficiency, high detection rates, and ultra-high timing resolution. *APL Photonics* **2017**,  
4 *2*, 111301.  
5  
6  
7  
8 (9) Boris, K. et al. Demonstration of sub-3 ps temporal resolution with a superconducting  
9 nanowire single-photon detector. *Nature Photonics* **2020**, *14*, 250–255.  
10  
11  
12 (10) Wu, J.; You, L.; Chen, S.; Li, H.; He, Y.; Lv, C.; Wang, Z.; Xie, X. Improving the  
13 timing jitter of a superconducting nanowire single-photon detection system. *Appl. Opt.*  
14 **2017**, *56*, 2195–2200.  
15  
16  
17  
18 (11) Huang, J.; Zhang, W.; You, L.; Zhang, C.; Lv, C.; Wang, Y.; Liu, X.; Li, H.; Wang, Z.  
19 High speed superconducting nanowire single-photon detector with nine interleaved  
20 nanowires. *Superconductor Science and Technology* **2018**, *31*, 074001.  
21  
22  
23  
24 (12) Müller, A. M.; Bardeen, C. J. Using a Streak Camera to Resolve the Motion of Molecular  
25 Excited States with Picosecond Time Resolution and 150 nm Spatial Resolution. *The*  
26 *Journal of Physical Chemistry C* **2007**, *111*, 12483–12489.  
27  
28  
29  
30 (13) Hamamatsu Photonics K.K., FESCA-100 Femtosecond streak camera. [https://www.hamamatsu.com/eu/en/product/photometry-systems/streak-camera/](https://www.hamamatsu.com/eu/en/product/photometry-systems/streak-camera/fesca-100-femtosecond-streak-camera/index.html)  
31 [fesca-100-femtosecond-streak-camera/index.html](https://www.hamamatsu.com/eu/en/product/photometry-systems/streak-camera/fesca-100-femtosecond-streak-camera/index.html), accessed 19 April 2020.  
32  
33  
34  
35  
36  
37  
38  
39 (14) Seifert, S.; van Dam, H. T.; Schaart, D. R. The lower bound on the timing resolution  
40 of scintillation detectors. *Physics in Medicine and Biology* **2012**, *57*, 1797–1814.  
41  
42  
43  
44 (15) Zhang, L.; Peng, W.; You, L. X.; Wang, Z. Superconducting properties and chemical  
45 composition of NbTiN thin films with different thickness. *Applied Physics Letters* **2015**,  
46 *107*, 122603.  
47  
48  
49  
50 (16) Zichi, J.; Chang, J.; Steinhauer, S.; von Fieandt, K.; Los, J. W. N.; Visser, G.;  
51 Kalthor, N.; Lettner, T.; Elshaari, A. W.; Zadeh, I. E.; Zwiller, V. Optimizing the sto-  
52  
53  
54  
55  
56  
57  
58  
59  
60

- 1  
2  
3  
4  
5  
6  
7  
8  
9  
10  
11  
12  
13  
14  
15  
16  
17  
18  
19  
20  
21  
22  
23  
24  
25  
26  
27  
28  
29  
30  
31  
32  
33  
34  
35  
36  
37  
38  
39  
40  
41  
42  
43  
44  
45  
46  
47  
48  
49  
50  
51  
52  
53  
54  
55  
56  
57  
58  
59  
60
- ichiometry of ultrathin NbTiN films for high-performance superconducting nanowire single-photon detectors. *Opt. Express* **2019**, *27*, 26579–26587.
- (17) Gourgues, R.; Los, J. W. N.; Zichi, J.; Chang, J.; Kalhor, N.; Bulgarini, G.; Dorenbos, S. N.; Zwiller, V.; Zadeh, I. E. Superconducting nanowire single photon detectors operating at temperature from 4 to 7 K. *Opt. Express* **2019**, *27*, 24601–24609.
- (18) Gourgues, R.; Zadeh, I. E.; Elshaari, A. W.; Bulgarini, G.; Los, J. W. N.; Zichi, J.; Dalacu, D.; Poole, P. J.; Dorenbos, S. N.; Zwiller, V. Controlled integration of selected detectors and emitters in photonic integrated circuits. *Opt. Express* **2019**, *27*, 3710–3716.
- (19) Gaudio, R.; op 't Hoog, K. P. M.; Zhou, Z.; Sahin, D.; Fiore, A. Inhomogeneous critical current in nanowire superconducting single-photon detectors. *Applied Physics Letters* **2014**, *105*, 222602.
- (20) O'Connor, J. A.; Tanner, M. G.; Natarajan, C. M.; Buller, G. S.; Warburton, R. J.; Miki, S.; Wang, Z.; Nam, S. W.; Hadfield, R. H. Spatial dependence of output pulse delay in a niobium nitride nanowire superconducting single-photon detector. *Applied Physics Letters* **2011**, *98*, 201116.
- (21) Zhao, Q.; Zhang, L.; Jia, T.; Kang, L.; Xu, W.; Chen, J.; Wu, P. Intrinsic timing jitter of superconducting nanowire single-photon detectors. *Applied Physics B* **2011**, *104*, 673–678.
- (22) You, L.; Yang, X.; He, Y.; Zhang, W.; Liu, D.; Zhang, W.; Zhang, L.; Zhang, L.; Liu, X.; Chen, S.; Wang, Z.; Xie, X. Jitter analysis of a superconducting nanowire single photon detector. *AIP Advances* **2013**, *3*, 072135.
- (23) Calandri, N.; Zhao, Q.-Y.; Zhu, D.; Dane, A.; Berggren, K. K. Superconducting nanowire detector jitter limited by detector geometry. *Applied Physics Letters* **2016**, *109*, 152601.

- 1  
2  
3 (24) Cheng, Y.; Gu, C.; Hu, X. Inhomogeneity-induced timing jitter of superconducting  
4 nanowire single-photon detectors. *Applied Physics Letters* **2017**, *111*, 062604.  
5  
6  
7  
8 (25) Li, P. A Review of Proximity Effect Correction in Electron-beam Lithography. *Arxiv*  
9 *preprint [cond-mat]* **2015**, arXiv: 1509.05169.  
10  
11  
12 (26) Cheng, R.; Guo, X.; Ma, X.; Fan, L.; Fong, K. Y.; Poot, M.; Tang, H. X. Self-aligned  
13 multi-channel superconducting nanowire single-photon detectors. *Opt. Express* **2016**,  
14 *24*, 27070–27076.  
15  
16  
17  
18 (27) Sidorova, M.; Semenov, A.; Hübers, H.-W.; Charaev, I.; Kuzmin, A.; Doerner, S.;  
19 Siegel, M. Physical mechanisms of timing jitter in photon detection by current-carrying  
20 superconducting nanowires. *Phys. Rev. B* **2017**, *96*, 184504.  
21  
22  
23  
24 (28) Liu, D.; Miki, S.; Yamashita, T.; You, L.; Wang, Z.; Terai, H. Multimode fiber-coupled  
25 superconducting nanowire single-photon detector with 70% system efficiency at visible  
26 wavelength. *Opt. Express* **2014**, *22*, 21167–21174.  
27  
28  
29  
30 (29) Li, H.; Zhang, L.; You, L.; Yang, X.; Zhang, W.; Liu, X.; Chen, S.; Wang, Z.; Xie, X.  
31 Large-sensitive-area superconducting nanowire single-photon detector at 850 nm with  
32 high detection efficiency. *Opt. Express* **2015**, *23*, 17301–17308.  
33  
34  
35  
36 (30) Wollman, E. E.; Verma, V. B.; Beyer, A. D.; Briggs, R. M.; Korzh, B.; Allmaras, J. P.;  
37 Marsili, F.; Lita, A. E.; Mirin, R. P.; Nam, S. W.; Shaw, M. D. UV superconducting  
38 nanowire single-photon detectors with high efficiency, low noise, and 4 K operating  
39 temperature. *Opt. Express* **2017**, *25*, 26792–26801.  
40  
41  
42  
43 (31) Chang, J.; Zadeh, I. E.; Los, J. W. N.; Zichi, J.; Fognini, A.; Gevers, M.; Doren-  
44 bos, S.; Pereira, S. F.; Urbach, P.; Zwiller, V. Multimode-fiber-coupled superconduct-  
45 ing nanowire single-photon detectors with high detection efficiency and time resolution.  
46 *Appl. Opt.* **2019**, *58*, 9803–9807.  
47  
48  
49  
50  
51  
52  
53  
54  
55  
56  
57  
58  
59  
60

- 1  
2  
3 (32) Allman, M. S.; Verma, V. B.; Stevens, M.; Gerrits, T.; Horansky, R. D.; Lita, A. E.;  
4 Marsili, F.; Beyer, A.; Shaw, M. D.; Kumor, D.; Mirin, R.; Nam, S. W. A near-  
5 infrared 64-pixel superconducting nanowire single photon detector array with integrated  
6 multiplexed readout. *Applied Physics Letters* **2015**, *106*, 192601.  
7  
8  
9  
10  
11 (33) Allmaras, J. P.; Beyer, A. D.; Briggs, R. M.; Marsili, F.; Shaw, M. D.; Resta, G. V.;  
12 Stern, J. A.; Verma, V. B.; Mirin, R. P.; Nam, S. W.; Farr, W. H. Large-Area 64-  
13 pixel Array of WSi Superconducting Nanowire Single Photon Detectors. Conference on  
14 Lasers and Electro-Optics. 2017; p JTh3E.7.  
15  
16  
17  
18  
19 (34) Miyajima, S.; Yabuno, M.; Miki, S.; Yamashita, T.; Terai, H. High-time-resolved 64-  
20 channel single-flux quantum-based address encoder integrated with a multi-pixel super-  
21 conducting nanowire single-photon detector. *Opt. Express* **2018**, *26*, 29045–29054.  
22  
23  
24  
25  
26 (35) Kuzmin, A.; Doerner, S.; Sidorova, M.; Wuensch, S.; Ilin, K.; Siegel, M.; Semenov, A.  
27 Geometrical Jitter and Bolometric Regime in Photon Detection by Straight Supercon-  
28 ducting Nanowire. *IEEE Transactions on Applied Superconductivity* **2019**, *29*, 1–5.  
29  
30  
31  
32 (36) Santavicca, D. F.; Adams, J. K.; Grant, L. E.; McCaughan, A. N.; Berggren, K. K.  
33 Microwave dynamics of high aspect ratio superconducting nanowires studied using self-  
34 resonance. *Journal of Applied Physics* **2016**, *119*, 234302.  
35  
36  
37  
38 (37) Zhao, Q.-Y.; Santavicca, D. F.; Zhu, D.; Noble, B.; Berggren, K. K. A distributed  
39 electrical model for superconducting nanowire single photon detectors. *Applied Physics*  
40 *Letters* **2018**, *113*, 082601.  
41  
42  
43  
44 (38) Dalacu, D.; Mnaymneh, K.; Lapointe, J.; Wu, X.; Poole, P. J.; Bulgarini, G.; Zwiller, V.;  
45 Reimer, M. E. Ultraclean Emission from InAsP Quantum Dots in Defect-Free Wurtzite  
46 InP Nanowires. *Nano Letters* **2012**, *12*, 5919–5923, PMID: 23066839.  
47  
48  
49  
50 (39) Versteegh, M. A. M.; Reimer, M. E.; Jöns, K. D.; Dalacu, D.; Poole, P. J.; Gulinatti, A.;  
51  
52  
53  
54  
55  
56  
57  
58  
59  
60

1  
2  
3 Giudice, A.; Zwiller, V. Observation of strongly entangled photon pairs from a nanowire  
4 quantum dot. *Nature Communications* **2014**, *5*, 5298.  
5  
6

7  
8 (40) Bulgarini, G.; Reimer, M. E.; Bouwes Bavinck, M.; Jöns, K. D.; Dalacu, D.;  
9 Poole, P. J.; Bakkers, E. P. A. M.; Zwiller, V. Nanowire Waveguides Launching Sin-  
10 gle Photons in a Gaussian Mode for Ideal Fiber Coupling. *Nano Letters* **2014**, *14*,  
11 4102–4106, PMID: 24926884.  
12  
13  
14

15  
16  
17 (41) Zadeh, I. E.; Elshaari, A. W.; Jöns, K. D.; Fognini, A.; Dalacu, D.; Poole, P. J.;  
18 Reimer, M. E.; Zwiller, V. Deterministic Integration of Single Photon Sources in Silicon  
19 Based Photonic Circuits. *Nano Letters* **2016**, *16*, 2289–2294.  
20  
21  
22  
23  
24  
25  
26  
27  
28  
29  
30  
31  
32  
33  
34  
35  
36  
37  
38  
39  
40  
41  
42  
43  
44  
45  
46  
47  
48  
49  
50  
51  
52  
53  
54  
55  
56  
57  
58  
59  
60

## For Table of Contents Use Only

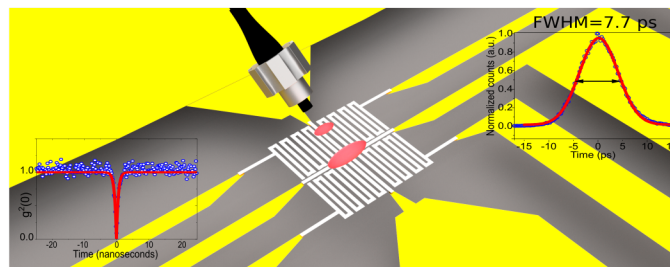


Figure 6: An illustration of a 4-pixel multimode fiber-coupled superconducting nanowire single-photon detector. Bottom left inset presents a photon antibunching measurement using two pixels with no beamsplitter. Top right inset shows time jitter measurement of an efficient fiber-coupled SNSPD achieving a time resolution of 7.7 ps.